Arabian Journal of Chemistry (2023) **16**, 104605

King Saud University

Arabian Journal of Chemistry

www.ksu.edu.sa
www.sciencedirect.com

ORIGINAL ARTICLE

Study on the corrosion inhibition of biomass carbon quantum dot self- aggregation on Q235 steel in hydrochloric acid

Siyuan Zheng [a,b], Li Feng [a,b,*], Zhiyong Hu [a,*], Jianan Li [a], Hailin Zhu [a], Xuemei Ma [a]

[a] *School of Chemical Engineering and Technology, North University of China, Taiyuan, Shanxi 030051, China*
[b] *Dezhou Graduate School, North University of China, Dezhou, Shandong 253034, China*

Received 16 November 2022; accepted 15 January 2023
Available online 23 January 2023

KEYWORDS

Biomass;
Carbon quantum dots;
Corrosion inhibitors;
Self-aggregation;
Electrochemistry

Abstract At present, the development of efficient green corrosion inhibitors has become one of the important directions of metal corrosion protection. In this paper, biomass carbon quantum dots (BCQDs) were prepared by hydrothermal reaction using biomass precursors. The optical properties and structural composition of the synthesized BCQDs were characterized in detail. After that, the corrosion inhibition performance of BCQDs was evaluated by EIS, Tafel, SEM and TEM. The electrochemistry and surface tests demonstrate that the aggregates can effectively prevent Q235 steel from corrosion in 1 M HCl medium at 298 K-328 K, with the maximum inhibition efficiency of 94.1 % at the concentration of 200 mg/L at 308 K. Finally, the corrosion inhibition mechanism was analyzed by FTIR, CA and XPS on the surface of the corroded carbon steel samples. The inhibition mechanism suggests that BCQDs can inhibit metal corrosion by self-aggregation and adsorption on metal surface. This is owing to its small size effect and functional groups containing heteroatoms, easily forming dense protective film.

1. Introduction

Carbon steel widely used in energy transportation, chemical, machining and other industries, has excellent ductility, thermal conductivity, electrical conductivity and other advantages. Unfortunately, rust will break the surface structure of carbon steel and reduce its performance, so the removal of oxides on the surface of carbon steel by pickling before use has become one of the indispensable processes (Wang et al., 2011; Verma et al., 2017). Hydrochloric acid is one of the main pickling in the industrial pickling process (Nadi et al., 2021). During pickling process, the acid removes the oxide from the surface of carbon steel but causes excessive corrosion of the metal, which results in huge economic and energy losses. Currently, a method of adding corrosion inhibitors to the pickling solution is applied to reduce excessive corro-

* Corresponding authors.
E-mail addresses: fengli_nuc@163.comhuz (L. Feng), hiyong@nuc.edu.cn (Z. Hu).

Peer review under responsibility of King Saud University.

Production and hosting by Elsevier

https://doi.org/10.1016/j.arabjc.2023.104605
1878-5352

sion of metal during the pickling process. Among the existing corrosion inhibitors, inorganic corrosion inhibitors such as chromates (de Damborenea et al., 2014) are cheap but more harmful to the environment, while organic corrosion inhibitors performing supper protective effect usually contain electron-rich groups and/or heterocyclic. Although the corrosion inhibition efficiency of organic inhibitors is remarkable, they mostly have the disadvantages of high toxicity, high cost and poor solubility in water (Murmu et al., 2019; Verma et al., 2016; Saha et al., 2016). With the development of the Times, the concept of sustainable development has been deepening, and the regulations of countries concerning the environment are becoming more perfect. Resulting the above corrosion inhibitors in the industrial process has been subject to many restrictions. Therefore, efficient green corrosion inhibitors have become the mainstream research orientation for corrosion protection researchers (Verma and Khan, 2015; Umoren and Eduok, 2016).

Carbon quantum dots (CQDs), as a new type of carbon material with the size below 10 nm, have inherent advantages of pretty hydrophilicity, excellent optical properties, excellent biocompatibility and low toxicity, etc., which are widely used in medical imaging, sensors and other fields (Ren et al., 2019; Xu et al., 2019; Sooksin et al., 2018; Niu et al., 2018). Based on the surface of CQDs is easily modified with functional groups, which gives CQDs more power and application. Also, they can form chemisorption with the metal surface, and is possible to agglomerate and deposit on the metal surface forming protective film (Cao et al., 2021; Yang et al., 2019). Theoretically, the thickness of the protective film formed by CQDs is larger than that formed by conventional organic corrosion inhibitors because of its self-aggregation.

Hence, CQDs as potentially efficient green corrosion inhibitors have attracted the attention of corrosion protection researchers. Cui et al. prepared CQDs by aminosalicylic acid and used CQDs them as corrosion inhibitors with an optimum corrosion inhibition rate of 96 %, demonstrating that CQDs exhibited excellent corrosion inhibition on carbon steel in acidic environments (Cui et al., 2017). Subsequently, Ye et al. synthesized *N*-CQDs, which were more effective for metal corrosion protection than CQDs without N elements (Ye et al., 2020). After then Zhu et al. synthesized N, S-CQDs by o-phenylenediamine and thiourea and further confirmed that the participation of S, N could greatly enhance the corrosion inhibition efficiency of CQDs (Guo et al., 2022). It is generally believed that the inhibitor molecules are bonded to the metal surface by chemisorption, physical adsorption, or complexation (de Damborenea et al., 2014; Quartarone et al., 2008). All these prove that the inhibition efficiency of CQDs from organics is affected by their chemical structure and the doping of heteroatoms can improve the inhibition efficiency. However, the current CQDs still use organic chemical reagents in the preparation process. The pollution of the environment by organic matter is not avoided from the source.

Since the grapefruit peels contain a large amount of organic substances such as amino acids and sugars, which provide carbon sources and doping elements for the synthesis of CQDs. Most importantly, they are low in toxicity, widely available, inexpensive and biocompatible. Given these facts, biomass carbon quantum dots (BCQD) have be synthesized as green corrosion inhibitors in this paper by hydrothermal reaction using grapefruit peel as a precursor. The morphology and composition of the synthesized BCQDs were characterized by Fourier transform infrared spectroscopy (FTIR), ultraviolet–visible spectrum (UV–vis), transmission electron microscope (TEM), X-ray photoelectron spectroscopy (XPS), X-ray Diffraction (XRD) and fluorescence spectrum (FS). And the corrosion inhibition efficiency of BCQDs at different concentrations and temperatures was also investigated by electrochemical tests (EIS ang Tafel curves tests). Furthermore, the corrosion inhibition mechanism of BCQDs from SEM, AFM, contact angle tests, XPS and FTIR was revealed to support the future development of BCQDs corrosion inhibitors.

2. Experimental details

2.1. Materials

The hydrochloric acid (36 %∼38 %) was purchased from Chengdu Kolon Reagent Factory and anhydrous ethanol (99.7 %) was purchased from Tianjin Damao Chemical Reagent Factory, both of which were of analytical purity grade. The carbon steel sheet used in this study was Q235 steel with the following chemical composition: C0.14 ∼ 0.22 %, Mn0.30 ∼ 0.65, Si ≤ 0.30, S ≤ 0.050, P ≤ 0.045, and Fe of the rest. Carbon steel was cut into 0.5 × 0.5 × 0.1 cm and 1 × 1 × 0.1 cm for a series of surface morphology and composition analysis. The samples for electrochemical tests were polished and sealed in epoxy resin to expose only 1 cm^2 of working area. The corrosion solution was 1 M hydrochloric acid with different concentrations of BCQDs.

2.2. Preparation of BCQDs

Firstly, the grapefruit peels were cleaned and dried in an oven at a constant temperature of 50 °C. The dried peels were subsequently crushed into powder using a grinder. The corresponding preparation process of BCQDs is shown in Fig. 1. 6 g grapefruit peel powder was dispersed in 180 ml deionized water stirring ultrasonically for 45 min to ensure its uniform dispersion. Then the mixture was transferred to a 300 ml polytetrafluoroethylene autoclave at 180 °C for 3 h (Lu et al., 2012). After the reaction was completed, the precipitate was removed by filtration, followed by placing the filtrate into a treated 1000 molecular weight Regenerated cellulose membrane tubing and dialyzing in deionized water for 48 h, with water changes every 6 h during this period. After that, the dialysate was collected and concentrated to 100 ml by a rotary evaporator. Finally, the concentrate was freeze-dried to obtain a powder of brown-black BCQDs and placed in a desiccator for use.

2.3. Characterization of BCQDs

The optical properties of BCQDs were characterized by a Lambda 35 UV spectrometer (UV) from PerkinElmer and a fluorescence spectrometer (FS) from Hitachi F-2700. The structures of BCQDs were analyzed by Scientifc Nicolet iS50 from Thermo test Fourier Transform Infrared Spectroscopy (FTIR) and Bruker-AXS/D8 ECO test X-ray Diffraction (XRD) from Bruker, Germany. And the content and species of BCQDs constituent elements and their chemical form were studied by X-ray photoelectron spectroscopy (XPS, ESCALAB250Xi) with a C1s peak of 284.8 eV. The particle size distribution, morphology and element composition of BCQDs were further observed by Transmission Electron Microscope (TEM) as well as Energy Dispersive Spectroscopy (EDS) using the Talos F200S transmission electron microscope from Thermo Fisher Scientific.

2.4. Corrosion electrochemistry measurements

The electrochemical data were measured by the CHI 710 electrochemical workstation of Shanghai Chenhua. And the test

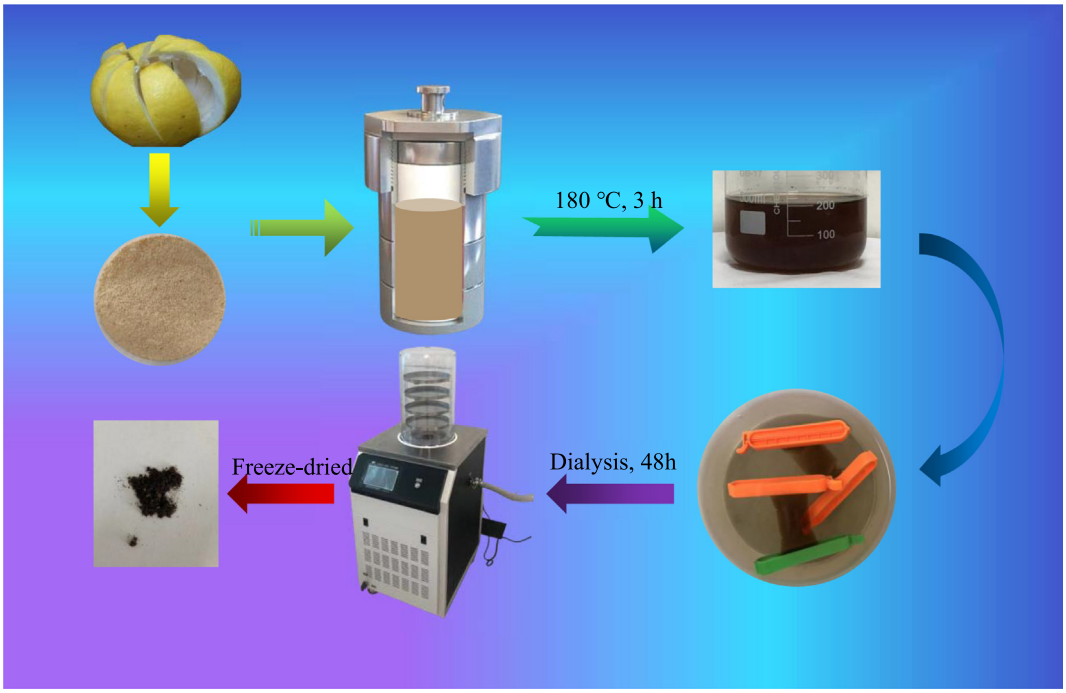

Fig. 1 Preparation process diagram of BCQDs.

system was a conventional three-electrode system. The auxiliary electrode was a platinum sheet electrode, the reference electrode was a saturated calomel electrode, and the working electrode was Q235 steel. Before testing, the surface of working electrode was polished to a mirror surface with 400#∼3000# waterproof abrasive paper and ultrasonically cleaned in ethanol solution, then dried by cold air. The corrosion solution was 1 M hydrochloric acid solution with different concentrations of BCQDs (0 mg/L, 25 mg/L, 50 mg/L, 100 mg/L and 200 mg/L for BCQDs). The open-circuit potential, electrochemical impedance spectroscopy and polarization curves were performed sequentially at a constant temperature of 298 K. The open-circuit potential (OCP) was tested for 1200 s. Within this time frame, the change in electrode potential was not exceed 3 mV, which determined that the system had reached stability. Subsequently, the electrochemical impedance spectra were tested in the frequency range of 0.01–100000 Hz, and the disturbance sinusoidal potential was a sinusoidal voltage of 5 mV. Finally, the polarization curves were tested for a polarization range of ± 250 mV based on the OCP with a scan rate of 1 mV/s. The formula for calculating corrosion inhibition efficiency by electrochemical testing is as follows (1–2) (Sudheer, 2013; Parthipan et al., 2021)

$$\eta(\%) = \frac{R_{ct} - R_{ct,0}}{R_{ct}} \times 100\% \quad (1)$$

$$\eta(\%) = \frac{i_{corr,0} - i_{corr}}{i_{corr,0}} \times 100\% \quad (2)$$

In the above equation, $i_{corr,0}$ and $R_{ct,0}$ are the corrosion current density and charge transfer resistance of the blank, respectively. The i_{corr} and R_{ct} are the corrosion current density and charge transfer resistance with various concentrations BCQDs.

2.5. Corrosion surface analysis (SEM, AFM and contact angle)

Scanning Electron Microscope (SEM, Japan Fe-SEM, JEOL-JSM-7800F), contact angle (Kruss DSA25s) and Atomic Force Microscope (AFM, Bruker, Dimension Icon) were used to test the corrosion morphology and hydrophobic properties of the Q235 sample surface after immersion in the corrosion solution at 298 K. Before testing, the samples were burnished to a mirror surface using 800#∼7000# water-grit sandpaper and ultrasonically cleaned by ethanol, dried with cold air and then immersed in 1 M hydrochloric acid solution with and without 200 mg/L BCQDs, respectively.

2.6. Inhibition mechanism (FTIR and XPS)

FTIR (Thermo, Scientifc Nicolet iS50) and XPS (Thermo, ESCALAB250Xi) are used to test the elemental content of the adsorbed layer on the carbon steel surface after corrosion. Before testing, the Q235 steel samples were treated in the same way as SEM, after which the treated Q235 steel was immersed in 1 M hydrochloric acid with and without 200 mg/L BCQDs, followed by testing of the Q235 sample surfaces by FTIR and XPS. They are used to study the interaction between BCQDs and carbon steel, supporting the corrosion inhibition mechanism of BCQDs. Before tests, the blank carbon steel samples were treated by the above.

3. Results and discussion

3.1. Characterization of BCQDs (UV, PL, XRD, FTIR)

The characterization results of BCQDs are shown in Fig. 2. It can be seen from XRD (Fig. 2(a)) crystal type results that the BCQDs are graphene-like structures. By comparison with the

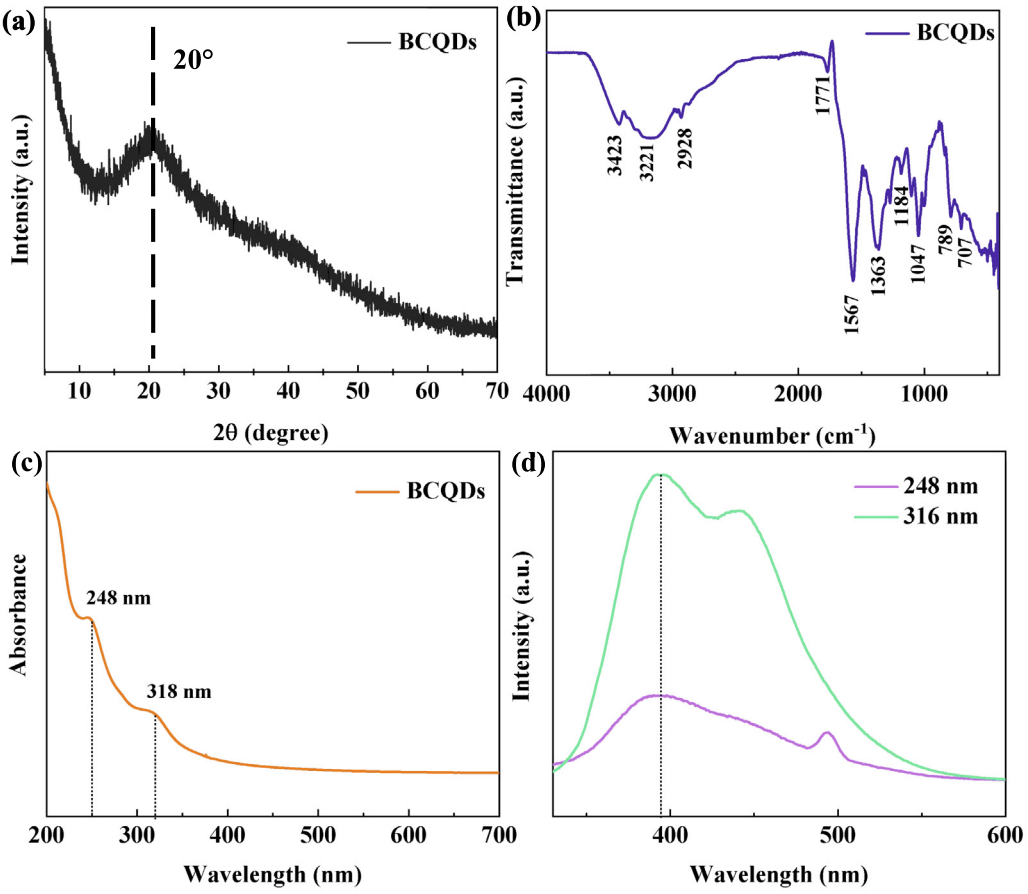

Fig. 2 Characterization result of BCQDs including XRD (a); FTIR (b); UV (c); and FS (d).

pdf card, this peak at 20° (2θ) is the peak of amorphous carbon (Wang et al., 2014). But the peak position relatively shifts to the left and widens, which may be caused by the effect of groups or doping of N and O elements on BCQDs.

Fig. 2(b) shows the FTIR information of BCQDs, from which it can be obtained that the sharp peaks at 3500 cm^{-1} to 3000 cm^{-1} are O—H and N—H. Broad peaks perhaps correspond to intramolecular hydrogen bonds (i.e. O—H and N—H after multimolecular titration). The absorption peak at 2929 cm^{-1} is attributed to C—H (–CH_3/–CH_2-) stretching vibration and the absorption peak at 1771 cm^{-1} is C═O stretching vibration. The peak at 1567 cm^{-1} is the C═C vibration in the benzene ring skeleton. The absorption peak at 1363 cm^{-1} is the C—N stretching vibration. The absorption peak at 1272 cm^{-1} is the C—O stretching vibration of the carboxylic acid. The peak at 1000–1475 cm^{-1} corresponds to C—H in-plane bending vibration and C—O stretching vibration, and 1000–650 cm^{-1} for C—H out-plane bending vibration (Qiang et al., 2019; Yang et al., 2014; Jiang et al., 2015; Hu et al., 2015; Song et al., 2017). The FTIR results indicate that the BCQDs contain a large number of N functional groups, O functional groups and unsaturated double bonds on the surface, which provides the potential efficient metal corrosion inhibition for BCQDs.

The UV results of BCQDs are illustrated in Fig. 2(c). BCQDs have two absorption peaks at 265 nm and 315 nm, respectively. The presence of C═O, N═O and other groups in the molecule can perform n-π* leaps, which requires less energy and absorb at wavelengths greater than 200 nm. From the results of FTIR and XPS, BCQDs contain a large amount of C═O, so the absorption at this position is mainly attributed to the n-π* leap of the C═O bonds, which also indicates that BCQDs contain more unsaturated bonds (Dong et al., 2012).

Fig. 2(d) shows the fluorescence spectra (FS) of BCQDs, it is not difficult to find that there are two emission peaks, which the emission wavelength of 393 nm – 440 nm formed the excitation wavelength of 316 nm and the emission wavelength of 393 nm-494 nm formed the excitation wavelength of 248 nm, respectively. In addition, the BCQDs solution emits light green fluorescence under the UV illumination of 345 nm (Wang et al., 2014; Jiang et al., 2015). This indicates that the BCQDs synthesized here have good photoluminescence properties.

3.2. TEM analysis of BCQDs

The morphology, constituent elements and average particle size of the BCQDs prepared in this paper were measured by TEM in Fig. 3. It shows the morphology (Fig. 3(a)), selected area electron diffraction (SAED) (Fig. 3(b)), the elemental composition (Fig. 3 (c)), and the information of particle size distribution (Fig. 3 (d)) of BCQDs.

In Fig. 3(a), it can be observed that BCQDs exhibit sheet-like aggregation and uniform spherical. A diffuse ring is evident from the selected area electron diffraction, which demon-

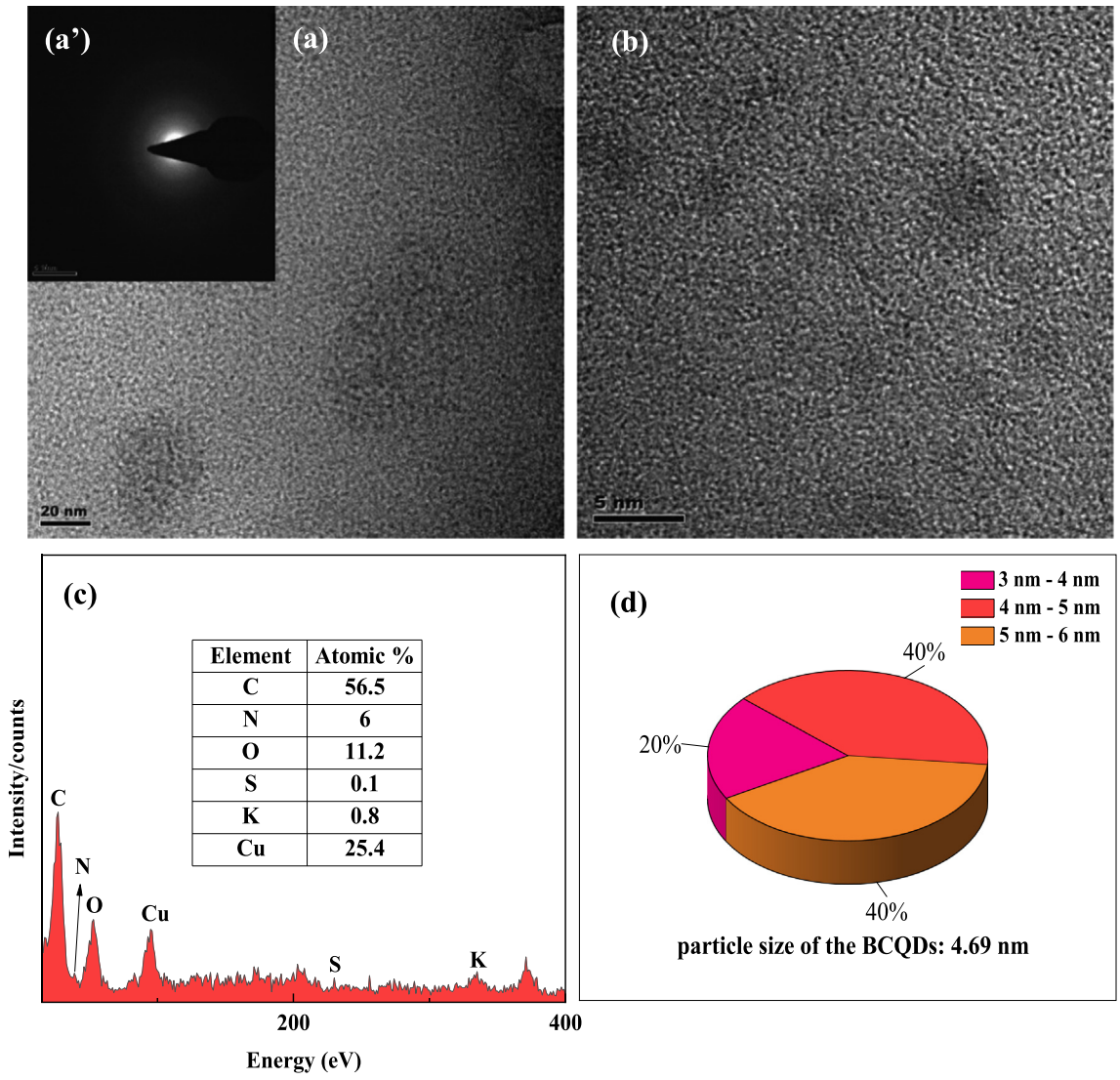

Fig. 3 TEM morphology (a)(b), SAED (a'), EDS (c) and size (d) results of BCQDs.

strates that the BCQDs prepared in this experiment are amorphous materials (Hao et al., 2011; Chin et al., 2010). This conclusion is consistent with the XRD results. In Fig. 3 (c), it demonstrates that the BCQDs composes of C, O, N, S and K elements. Here, Cu is detected due to the copper mesh used in the TEM test. This result also indicates that the heteroatoms in the biomass precursors are effectively doped into the BCQDs. Fig. 3 (d) is the particle size distribution of BCQDs, which also suggests that the particle sizes of BCQDs range from 3 nm to 6 nm and the average particle size is 4.69 nm. The smaller particle size contributes to the increased denseness of the protective layer formed by BCQDs on the surface of carbon steel. Moreover, the smaller particle size makes the nanoparticles have higher surface energy, which makes them easy to aggregate in the solution. This property may make the protective layer of BCQDs on the carbon steel surface thicker and more dense than the adsorption film of conventional organic corrosion inhibitors, which can better isolate the carbon steel from the contact with the corrosion solution.

3.3. XPS analysis of BCQDs

Fig. 4 shows the survey and high-resolution XPS spectrum of BCQDs. From the survey spectrum (Fig. 4 (a)), the main constituent elements of BCQDs are C (66.52 %), O (29.50 %), N (2.75 %), P (0.80 %) and S (0.43 %), respectively. High C and O content, which is attributed to the grapefruit peel contains more sugars and flavonoids, etc.

Obviously, in C1s high-resolution XPS spectrum (Fig. 4 (b)), four binding energy peaks at 288.8 eV, 287 eV, 286 eV and 284.3 eV can be observed, and their corresponding components are O-C═O, C═N, C─O/C─N and C─C/C─H, respectively (Xu et al., 2014; Roy et al., 2015). Fig. 4 (c) shows the O1s high-resolution XPS spectrum. The peak position at 533 eV corresponds to C═O, and the peak appearing at 531.5 eV corresponds to C─O (Xu et al., 2014; Hulicova-Jurcakova et al., 2009). Besides, Fig. 4 (d) is the high-resolution XPS spectrum of N1s, by fitting, the peak at

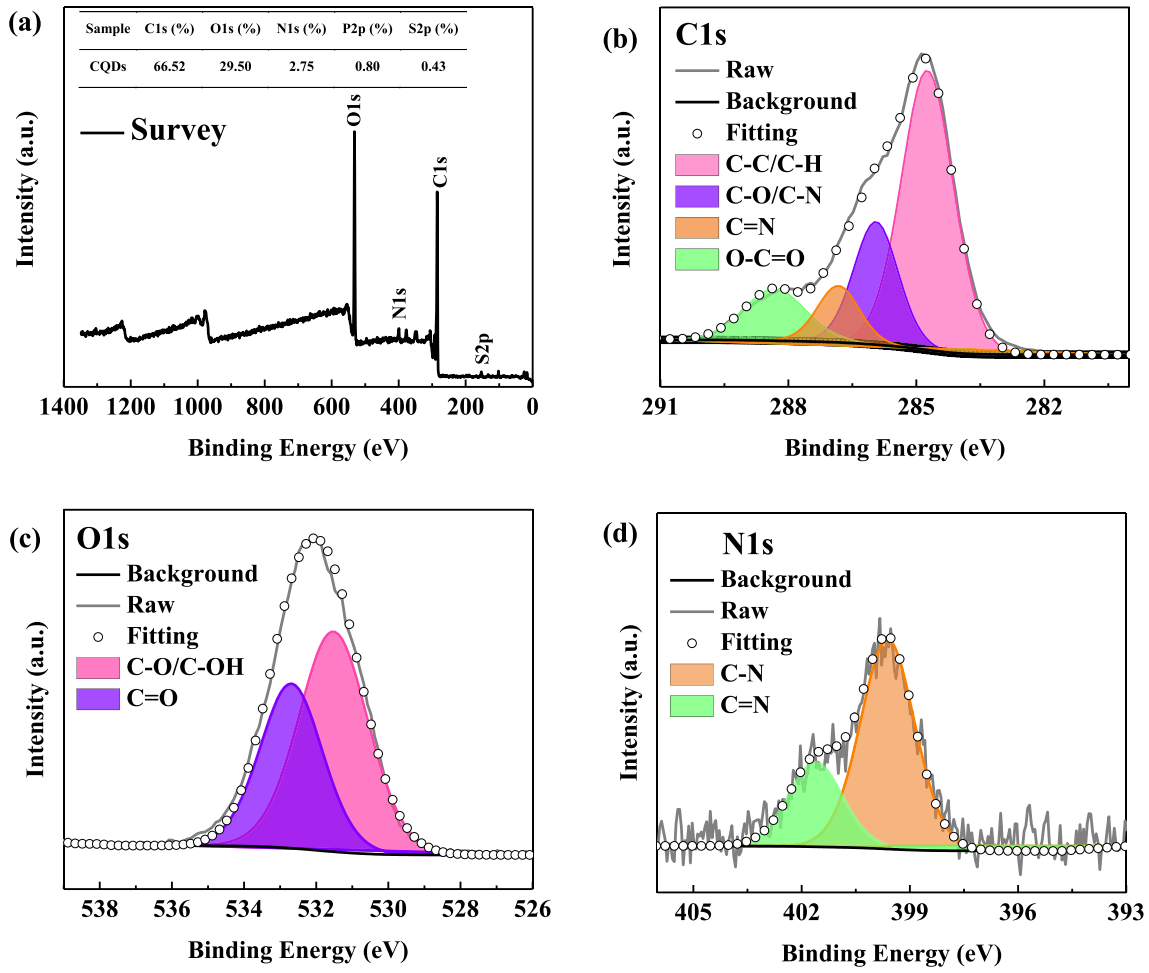

Fig. 4 The survey and high-resolution (C1s, O1s and N1s) XPS spectrum of BCQDs.

401.3 eV is C═N, and the peak appearing at 399.7 eV corresponds to C─N (Yang et al., 2014; Xu et al., 2014).

As a result, the N, O and other heteroatoms in grapefruit peel are effectively doped into the BCQDs forming abundant functional groups and unsaturated bonds on the surface of BCQDs, which is consistent with the FTIR test results. It makes BCQDs chemisorb on the carbon steel surface more easily, thus improving the corrosion inhibition performance.

3.4. Effect of concentration

The electrochemical open circuit potential, polarization curve and impedance spectrum results of Q235 steel in 1 M hydrochloric acid containing different concentrations of BCQDs at 298 K are shown in Fig. 5. The relevant data are listed in Table 1 and Table 2. The electrochemical impedance spectrum data were fitted by ZsimpWin software using the equivalent circuit (Fig. 6), where R_s is the solution resistance, R_{ct} is the charge transfer resistance, and *CPE* is the constant phase angle original expressed by equation (Popova et al., 2003; Ren et al., 2022):

$$Z_{\mathrm{CPE}} = \frac{1}{Y_0(j\omega)^n} \tag{3}$$

In the above equation, j is an imaginary unit, w is the angular frequency, and n is the dispersion effect index. The n represents the surface roughness and inhomogeneity of the working surface of the working electrode, ranging from −1 to 1. The closer n is to 1, the closer the *CPE* is to the pure capacitance. The value of C_{dl} can be calculated by the following equation (Sanaei et al., 2019):

$$C_{\mathrm{dl}} = Y_0(\omega)^{n-1} = Y_0(2\pi f_{Zim-Max})^{n-1} \tag{4}$$

In Fig. 5 (a), the Nyquist plots consists of the capacitive loops. The radius of the capacitive loops grows as the concentration of BCQDs increases, also the charge transfer resistance shows an increasing trend at the same time. This indicates that the corrosion of working electrode is inhibited effectively. And corrosion inhibition efficiency of BCQDs becomes more powerful as the concentration increases. Additionally, the Bode plots (Fig. 5 (b)) also show that the phase angle and impedance modulus increase with the increase of corrosion inhibitor concentration, which also indicates that the concentration has a great positive effect on the corrosion inhibition efficiency of BCQDs. Meanwhile, the shape of the impedance arc does not change as the radius of impedance increases, which means that the added concentration of BCQDs has no influence on the corrosion mechanism (Qiang et al., 2018; Qiang et al., 2018).

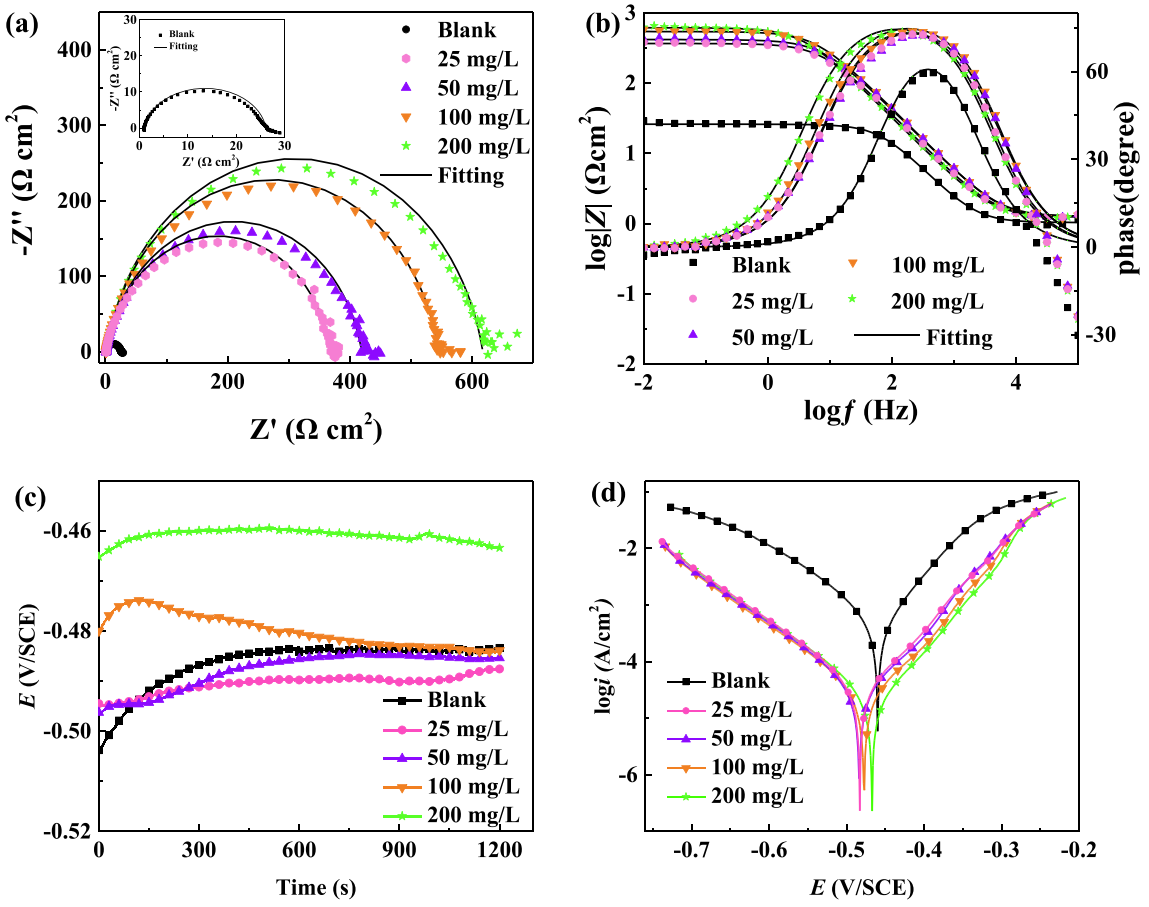

Fig. 5 The electrochemical Nyquist (a), Bode (b) plots, open circuit potential (c), and polarization curves (d) of Q235 steel in 1 M hydrochloric acid with different concentrations of BCQDs at 298 K.

Table 1 The parameters for electrochemical impedance spectrum with different concentrations of BCQDs at 298 K.

	C (mg/L)	R (Ω cm^2)	$Y_0 \times 10^{-5}$ (Ω cm^2)	n	C_{dl} (μFcm^{-2})	R_{ct} (Ω cm^2)	η_E (%)
Blank	0	1.036	15.950	0.917	96.46	25.07	–
CQDs	200	1.254	7.135	0.883	48.47	616.30	95.9
	100	1.226	7.419	0.888	49.98	544.20	95.4
	50	1.260	8.169	0.879	51.85	418.30	94.0
	25	1.263	9.172	0.886	58.48	367.40	93.2

Table 2 The parameters for polarization curves with different concentrations of BCQDs at 298 K.

	C (mM)	E_{ocp} (mV/SCE)	E_{corr} (mV/SCE)	i_{corr} (A cm^{-2})	β_c (mV dec^{-1})	β_a (mV dec^{-1})	η_T (%)
Blank	0	−482.9	−468.8	4.872×10^{-4}	−92.39	146.49	–
CQDs	200	−465.6	−467.0	2.089×10^{-5}	−96.54	166.17	95.7
	100	−483.9	−477.1	2.348×10^{-5}	−96.61	163.57	95.2
	50	−485.4	−483.3	2.812×10^{-5}	−97.56	166.80	94.2
	25	−487.6	−479.6	3.177×10^{-5}	−98.39	163.14	93.5

From the data in Table 1, the value of charge transfer resistance (R_{ct}) increases with the concentration of BCQDs, which is owing to the formation of a protective film on the metal surface by BCQDs increasing the resistance to electron exchange between the solid phase and the liquid phase. And the value of the bilayer capacitance (C_{dl}) decreases, because the BCQDs film on the metal surface isolates the contact between the metal and water molecules. At the same time, the corrosion inhibi-

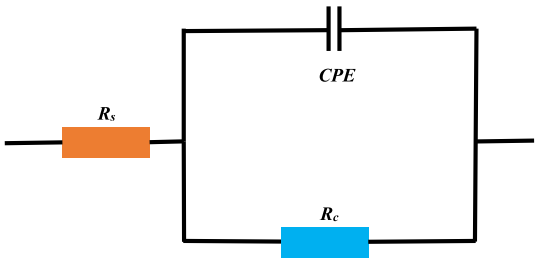

Fig. 6 The equivalent circuit fitting the electrochemical impedance spectrum results.

tion efficiency (η) increases with increasing concentration, and the maximum corrosion inhibition efficiency reaches more than 95 % when the concentration of BCQDs is 200 mg/L.

Fig. 5 (c) shows the open circuit potential of Q235 steel in 1 M hydrochloric acid with the addition of different concentrations of BCQDs. Compared to the blank, with the increase of BCQDs concentration, the open circuit potential first decreases and then increases, which may be due to the adsorption or/and aggregation of BCQDs. Meanwhile, the open circuit potential stabilization time was significantly shortened with the increase of BCQDs concentration, which indicates that the increase of concentration is beneficial to the rapid film formation of BCQDs on the Q235 surface. Fig. 5 (d) shows the polarization curves of Q235 steel in 1 M hydrochloric acid containing different concentrations of BCQDs. It is clear that the corrosion current density decreases significantly compared to the blank, with the addition of BCQDs. Moreover, the polarization curves show a decrease in both the anode and cathode of the polarization curves, which implies that the BCQDs as mixed corrosion inhibitors perform a significant inhibitory effect on both the cathodic and anodic reactions. By comparing the polarization curves of each concentration, it is found that the graphical pattern does not change significantly with the increase of BCQDs concentration, which demonstrates that the change of concentration does not lead to the alteration of the corrosion inhibition mechanism.

Table 2 shows the data of the polarization curves from linear extrapolation method. The data shows that the corrosion potential has a trend of negative shift followed by positive shift with the gradual addition of corrosion inhibitor. The current density decreases significantly due to the addition of corrosion inhibitor, which suggests that the corrosion tendency of Q235 steel is suppressed with the addition of BCQDs. The corrosion inhibition efficiency reaches up to more than 95 % when the concentration of BCQDs is 200 mg/L, which is consistent with the impedance results. Simultaneously, analysis of the data reveals that the change of corrosion potential of BCQDs was less than 85 mV compared with that of the blank control, further presenting the BCQDs synthesized in this study are mixed corrosion inhibitors (Zheng et al., 2015; Guo et al., 2023).

3.5. *Effect of temperature*

Fig. 7 shows the Nyquist plots and polarization curves of Q235 steel in 1 M hydrochloric acid containing 200 mg/L BCQDs at different temperatures (298 K, 308 K, 318 K and 328 K). The relevant data are listed in Table 3 and Table 4.

Observation of the Nyquist plots reveal that the radius of the capacitive loops radius decreases significantly with increasing temperature for both added BCQDs and the blank. It demonstrates that the change of temperature has a great influence on the corrosion inhibition efficiency of BCQDs, and the corrosion rate of metals is accelerated at high temperatures (Qiang et al., 2017). In addition, it is found from the Bode plots that the impedance modulus and phase angle gradually decrease with increasing temperature for all plots, but the BCQDs still exhibit excellent corrosion inhibition performance compared to the blank.

Table 3 shows the impedance data at different temperatures. Clearly, R_{ct} of BCQDs decreases gradually with the increase of temperature, which may make the BCQDs covered on the metal surface become loose due to worse adsorption ability of BCQDs caused by the increase of temperature. Meanwhile, the R_{ct} of the blank control group also shows a decreasing trend, which is caused by the accelerated corrosion rate of the metal in the hydrochloric acid solution with the increasing temperature. Secondly, the corrosion inhibition efficiency of BCQDs performs a increasing trend and then decreasing with the increase of temperature, and the highest

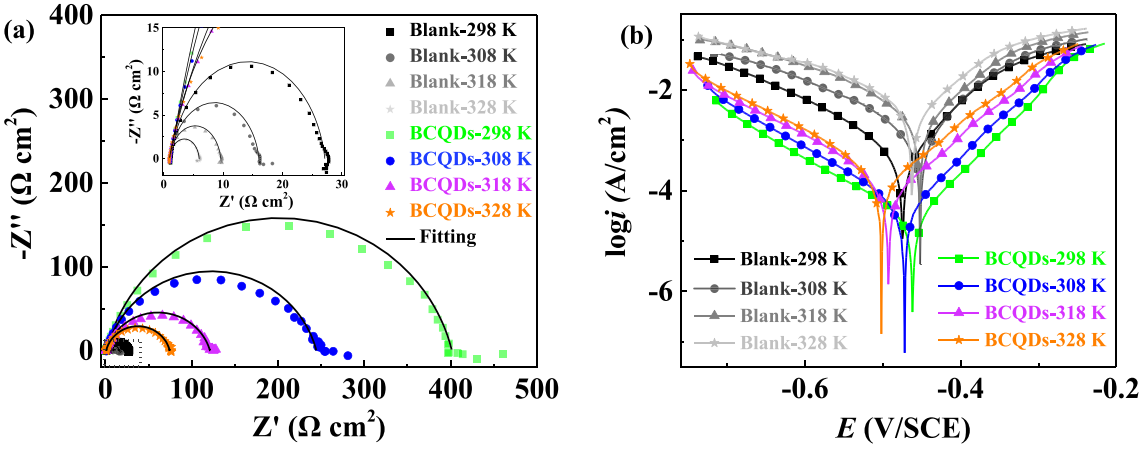

Fig. 7 The Nyquist plots (a) and polarization curves (b) of Q235 steel in 1 M hydrochloric acid with 200 mg/L BCQDs at various temperature.

Table 3 The parameters for EIS with 200 mg/L BCQDs at different temperature.

Temperature	R (Ω cm^2)	$Y_0 \times 10^{-5}$ (Ω cm^2)	n	C_{dl} (μFcm^{-2})	R_{ct} (Ω cm^2)	η_E (%)
298 K						
Blank	1.266	15.28	0.904	85.41	25.90	–
BCQDs	1.140	9.15	0.852	51.01	400.30	93.5
308 K						
Blank	1.147	18.98	0.907	104.47	14.88	–
BCQDs	1.093	10.56	0.841	53.04	256.40	94.1
318 K						
Blank	1.015	22.52	0.917	127.77	8.58	–
BCQDs	1.012	13.79	0.825	58.44	120.20	93.0
328 K						
Blank	1.002	23.49	0.939	151.33	5.51	–
BCQDs	0.976	11.62	0.853	50.45	73.56	92.5

Table 4 The parameters for polarization with 200 mg/L BCQDs at different temperature.

Temperature	E_{corr} (mV/SCE)	i_{corr} (A cm^{-2})	β_c (mV dec^{-1})	β_a (mV dec^{-1})	η_T (%)
298 K					
Blank	−475.0	5.242×10^{-4}	−84.83	130.46	–
BCQDs	−462.0	3.239×10^{-5}	−82.30	157.84	93.8
308 K					
Blank	−452.0	1.361×10^{-3}	−67.67	112.37	–
BCQDs	−472.0	4.646×10^{-5}	−90.65	161.52	96.5
318 K					
Blank	−453.0	3.101×10^{-3}	−72.43	113.83	–
BCQDs	−493.0	1.197×10^{-4}	−87.28	146.43	96.1
328 K					
Blank	−463.0	5.181×10^{-3}	−65.56	106.10	–
BCQDs	−502.0	2.132×10^{-4}	−86.25	137.04	95.94

corrosion inhibition efficiency (93.9 %) is achieved when the temperature reaches 308 K. This may be due to the fact that the increase in temperature not only promotes the corrosion of metals, but also accelerates the movement of BCQDs in solution, which improves the rapid formation of protective films on metal surfaces. However, when the temperature rises again, the increase in the rate of metal corrosion exceeds the rate of increase in corrosion inhibition performance owing to the accelerated movement of BCQDs, and the excessive temperature may lead to the weakened adsorption capacity of BCQDs on the surface of Q235 steel resulting in desorption, thus a decrease in corrosion inhibition efficiency.

In polarization curves (Fig. 7 (b)), the corrosion current density is significantly lower with the addition of BCQDs compared to the blank at each temperature. This suggests that the increase in temperature accelerates the corrosion of Q235 steel in hydrochloric acid medium, BCQDs are still efficient in inhibiting the corrosion. Besides, the type of corrosion inhibition of BCQDs is not changed.

Table 4 shows the relevant polarization curve data obtained by the linear extrapolation method. As the temperature rises, the corrosion current density increases and the corrosion potential shifts negatively. The corrosion inhibition efficiency shows a trend of increasing first and then decreasing, with the highest corrosion inhibition efficiency of BCQDs reaching 96.6 % at the temperature of 318 K. It presents that BCQDs still have excellent corrosion inhibition performance after increasing the temperature, which may be caused by the accelerated movement rate of BCQDs in the solution. Meanwhile, the temperature increase does not change the corrosion inhibition mechanism of BCQDs. In summary, the corrosion inhibition efficiency of the BCQDs synthesized in this study was not greatly affected after increasing the temperature. This advantage is different from conventional organic corrosion inhibitors, so BCQDs are suitable as high-temperature corrosion inhibitors.

3.6. Corrosion appearance analysis

Fig. 8 and Fig. 9 respectively show SEM and AFM images of Q235 steel after immersion in 1 M hydrochloric acid solution with and without BCQDs at the temperature of 298 K for 24 h. Fig. 8 ((a-1), (a-2), (a-3), (b-1), (b-2), (b-3)) shows the mapping of EDS. The comparison of the images from SEM shows that the samples in the blank solution are severely eroded, while the samples in the solution with BCQDs perform fewer surface erosion marks. This further confirms that the BCQDs prepared in this work can effectively inhibit the corrosion of Q235 steel in hydrochloric acid environment. In the mapping images of the blank samples, there is a large accumulation of carbon element where the metal is heavily corroded, while the images of the samples with BCQDs shows a uniform

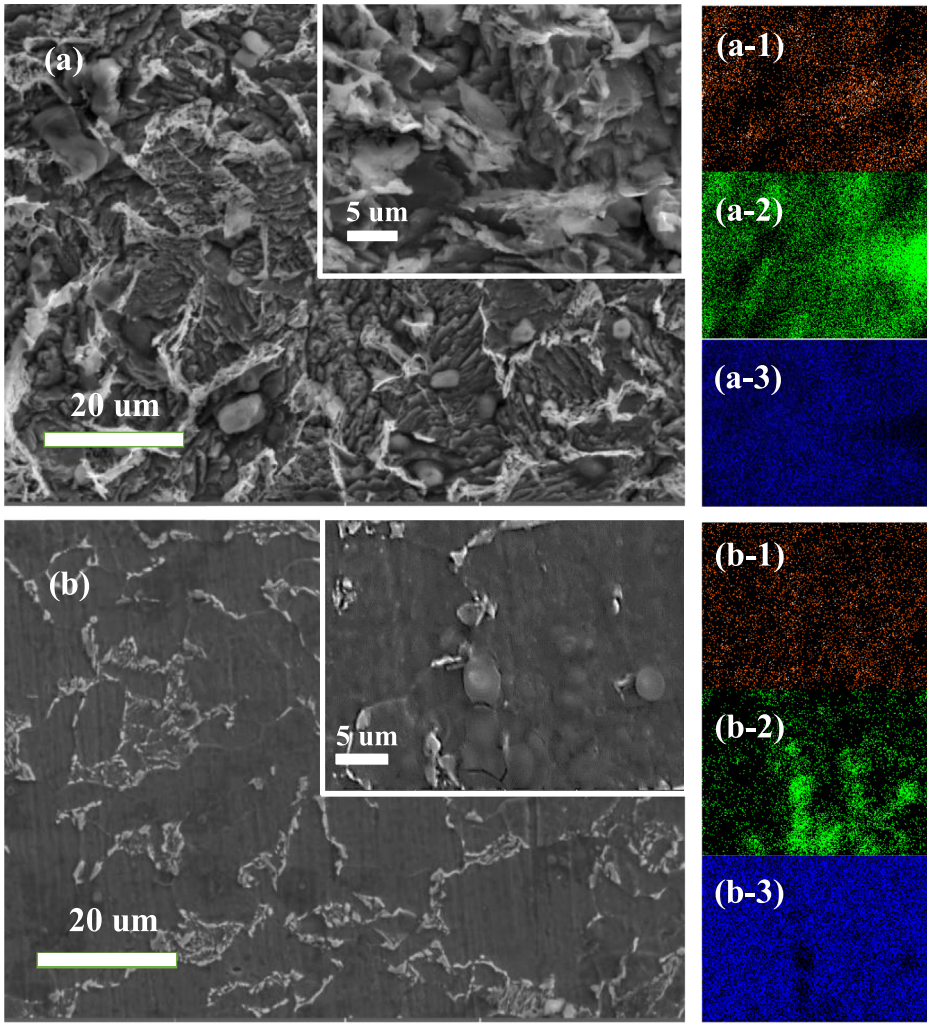

Fig. 8 SEM corrosion morphology and element distribution of Q235 steel in various solutions (a) blank; (b) BCQDs-200 mg/L; (a-1) mapping of C for blank; (a-2) mapping of O for blank; (a-3) mapping of Fe for blank; (b-1) mapping of C for BCQDs-200 mg/L; (b-2) mapping of O for BCQDs-200 mg/L; (b-3) mapping of Fe for CQDs-200 mg/L.

distribution of carbon elements. The severe erosion of Q235 steel in hydrochloric acid solution resulted in the exposure of carbon elements in the metal to the surface. For the mapping of oxygen elements, the samples with BCQDs appear to have less oxygen elements compared to the blanks. This situation is attributed to the exposure of the samples to air during testing making it produce iron oxides, while the samples treated with BCQDs are not easily oxidized in air due to the protective film of BCQDs attached to its surface.

Fig. 9 is the 3D map and the diagonal height plot of the AFM of Q235 steel after immersion in 1 M hydrochloric acid with and without BCQDs for 4 h. This test shows the surface roughness of carbon steel after being corroded by hydrochloric acid, and judges the corrosion inhibition effect of the corrosion inhibitor by the surface roughness. Q235 steel is severely corroded in 1 M hydrochloric acid without BCQDs, and its average roughness (R_a) is 127.952 nm. when BCQDs are added, the average roughness of Q235 steel was reduced to 15.231 nm, and its surface is smooth in the 3D map compared with the control group without BCQDs. The above phenomenon shows that the corrosion of Q235 steel in 1 M hydrochloric acid is effectively suppressed with the addition of BCQDs.

3.7. Surface composition analysis

Fig. 10 shows the sample surface FTIR spectrum of Q235 samples immersion in 1 M hydrochloric acid added with 200 mg/L of BCQDs after 12 h and the contact angle of Q235 samples immersion in 1 M hydrochloric acid with and without 200 mg/L of BCQDs after 12 h, respectively. By comparing the contact angle information, the hydrophobic property of the sample with BCQDs is significantly improved compared to the blank. The reason may be that BCQDs containing heterocyclic or heteratomic groups are physically or chemically adsorbed on the surface of Q235 steel, forming a protective film that changes the surface morphology and enhances the hydrophobicity of the sample surface. Therefore, it is possible to effectively isolate the contact between the corrosion solution and the metal, which effectively enhances the corrosion inhibition performance.

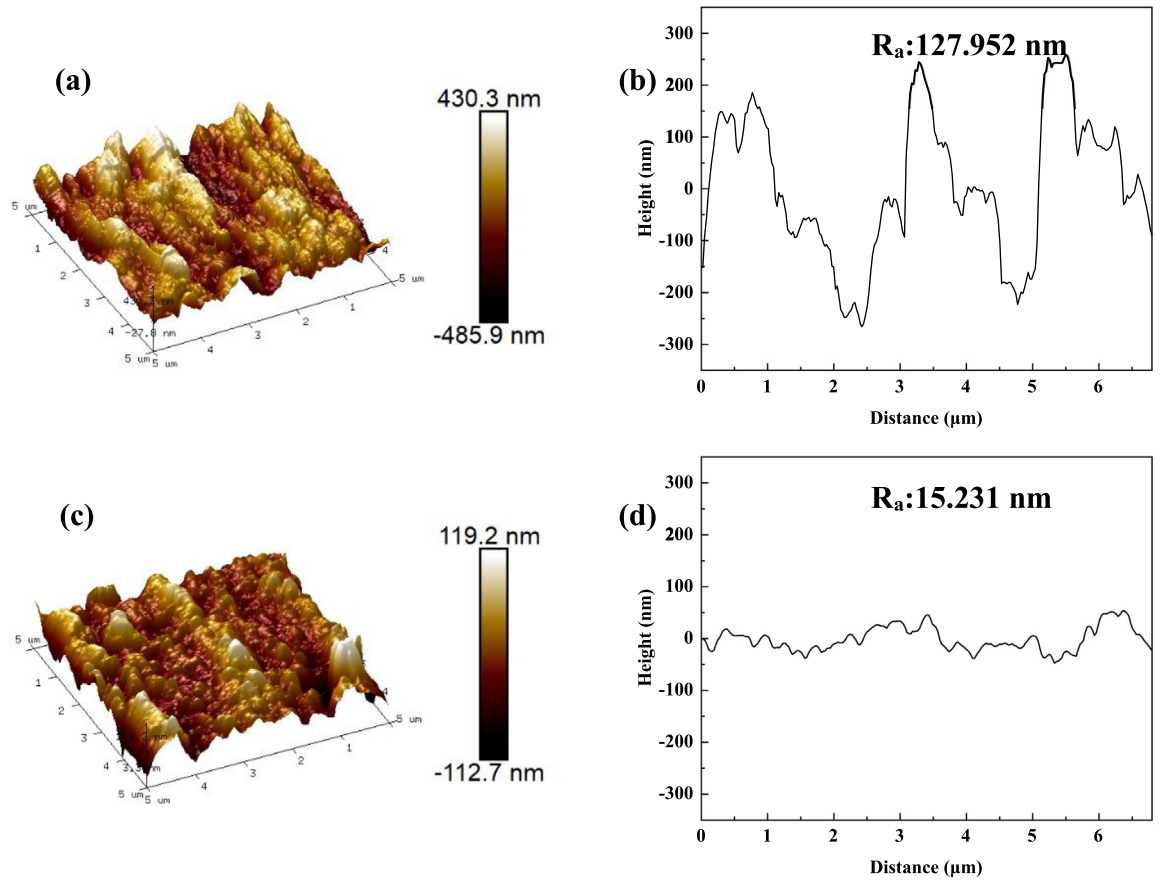

Fig. 9 AFM morphology and height plots of samples after corrosion, blank sample (a, b); BCQDs-treated sample (c, d).

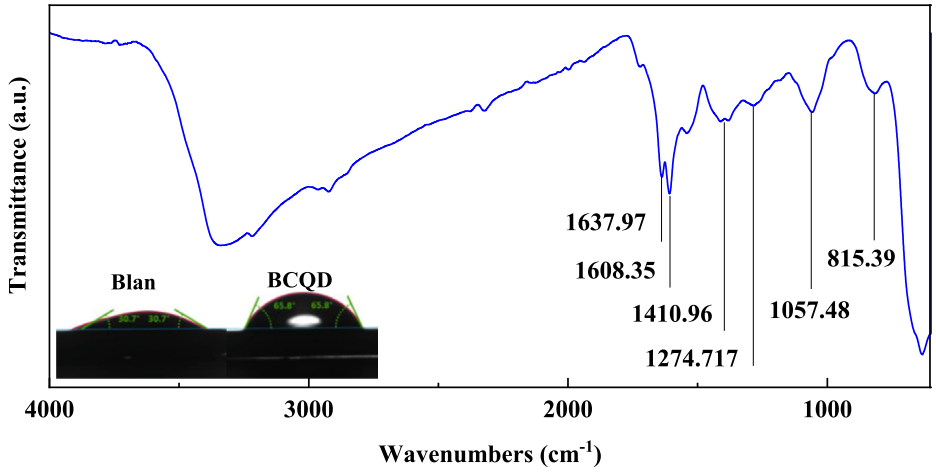

Fig. 10 FTIR spectrum of Q235 samples with 200 mg/L of BCQDs and the contact angle of Q235 samples with and without 200 mg/L of BCQDs after 12 h.

As shown in the FTIR, the sharp peaks at 3500 cm^{-1} to 3000 cm^{-1} are O—H and N—H. Broad peaks perhaps correspond to intramolecular hydrogen bonds (i.e. O—H and N—H after multimolecular titration). The peak at 1637.92 cm^{-1} is C═O stretching vibration. The peak at 1608.35 cm^{-1} is the C═C vibration in the benzene ring skeleton. 1410.96 cm^{-1} is a characteristic peak of C—N stretching vibration. The absorption peak at 1274.717 cm^{-1} is the C—O stretching vibration of the carboxylic acid. The peak at 1000–1475 cm^{-1} corresponds to C—H in-plane bending vibration and C—O stretching vibration, and 1000–650 cm^{-1} for C—H out-plane bending vibration. The characteristic peaks were detected in comparison with the FTIR results of BCQDs powder, which indicates that BCQDs aggregates were success-

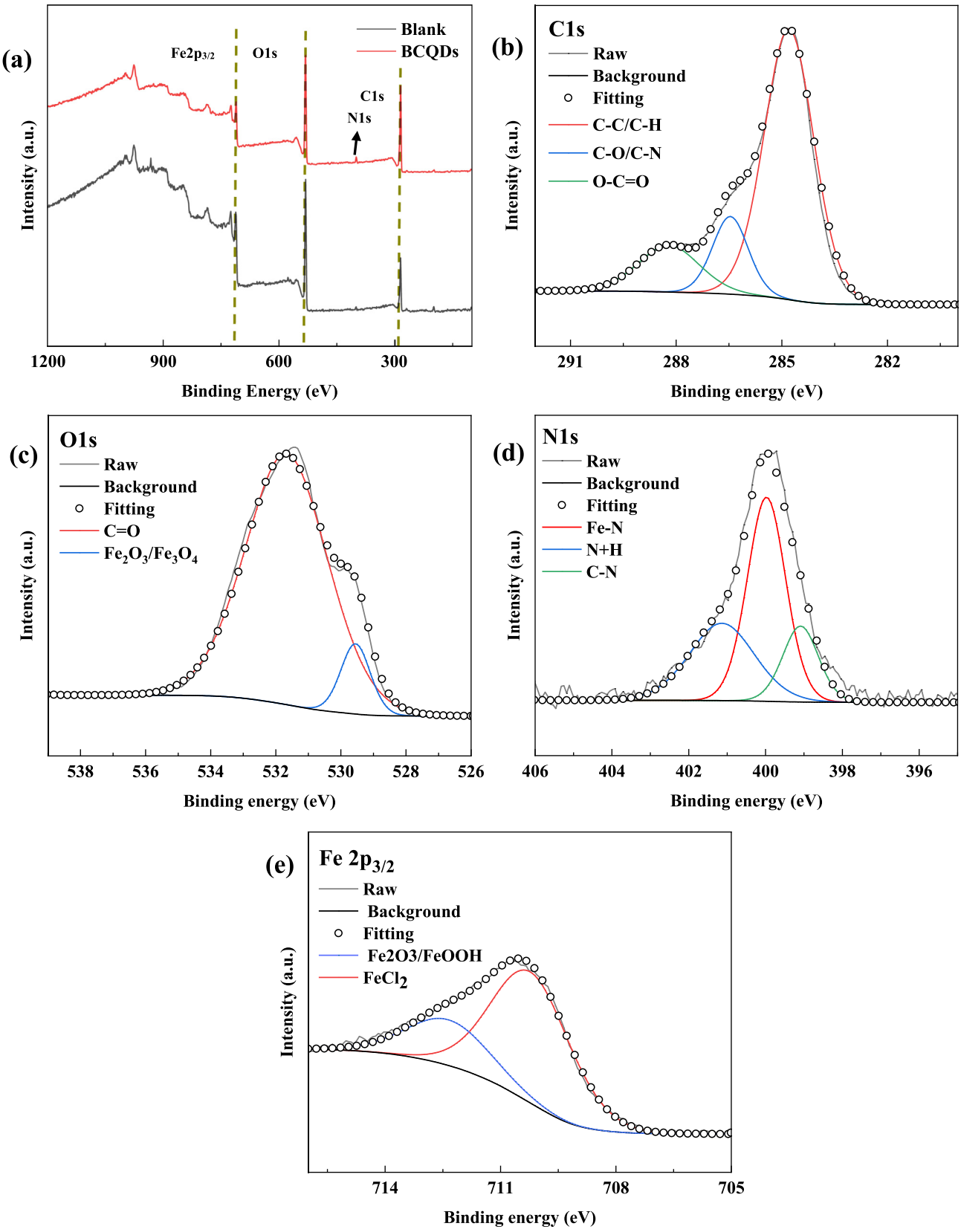

Fig. 11 XPS test results of Q235 steel immersed in 1 M hydrochloric acid with and without 200 mg/L of BCQDs for 24 h; (a)The survey XPS spectrum of Blank and BCQDs; high-resolution (C1s (b), O1s (c), N1s (d) and $Fe2p_{3/2}$ (e)) XPS spectrum of BCQDs.

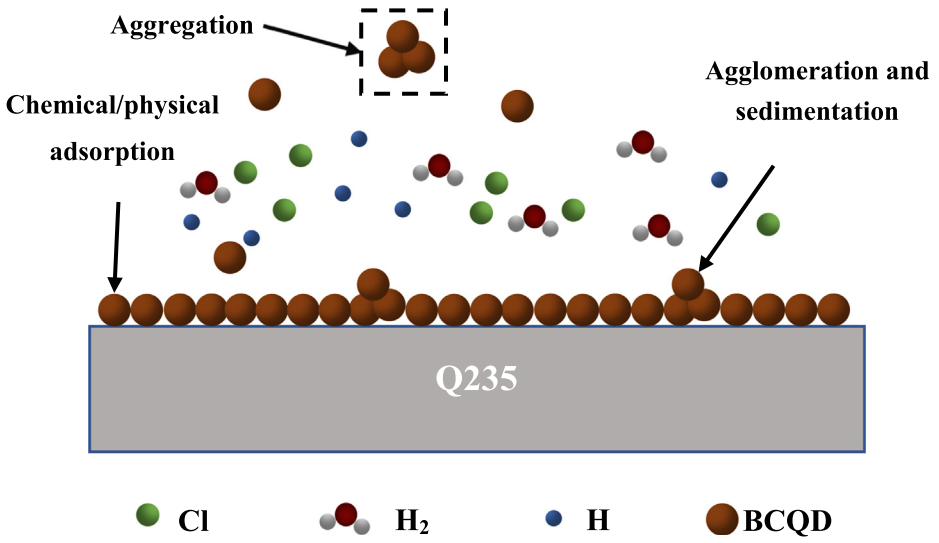

Fig. 12 Protection mechanism of BCQDs on Q235 carbon steel in 1 M hydrochloric acid solution.

fully adsorbed onto the surface of carbon steel. However, compared with the characteristic peaks of the BCQDs powder, the characteristic peaks of the carbon steel surface are relatively weaker, and the peak positions are slightly displaced, which is owing to de the aggregation and/or adsorption chemically of BCQDs.

From the contact angle results, the contact angle of the carbon steel samples soaked in hydrochloric acid without corrosion inhibitor is 30.7°, but the contact angle of the carbon steel samples soaked in hydrochloric acid solution with 100 mg/L BCQDs reached 65.8°. This indicates that the hydrophobic property of the carbon steel surface is changed with the addition of BCQDs. Combined with the XPS and FTIR analysis of the carbon steel surface after immersion, the reason may be that BCQDs form a protective film on the carbon steel surface by chemical and physical adsorption. This improves the hydrophobic properties of the carbon steel surface and effectively isolates the corrosive medium from the carbon steel surface. As a result, this protective film effectively isolates the corrosive medium from the carbon steel surface by improving the hydrophobic properties of the carbon steel surface, thus improving the corrosion inhibition effect.

Furthermore, Fig. 11 shows the XPS test results of Q235 steel immersed in 1 M hydrochloric acid with and without 200 mg/L of BCQDs for 24 h. Fig. 11(a) shows the XPS survey spectrum of the blank sample and the sample with BCQDs film. Fig. 11 (b), (c), (d) and (e) show the high-resolution XPS spectrum of C1s, O1s, N1s and Fe 2p of the samples spiked with BCQDs, respectively.

The information in Fig. 11(a) shows that element N was detected on the surface of the sample with BCQDs compared to the blank sample, which indicates that the BCQDs formed the protective film on the surface of the carbon steel. In addition, the elemental content of the samples with and without BCQDs showed an increase in the elemental content of C and decrease in the elemental content of O and Cl, which indicates that the adsorption of BCQDs on the surface of carbon steel to form a film effectively slows down the corrosion of metals by Cl^- in corrosion solution and O_2 in the air.

In Fig. 11 (b), the peaks at 284.80 eV, 286.46 eV and 288.28 eV correspond to the components C—C/C—H, C—O/C—N and O-C=O, respectively (Zhu et al., 2022). The two peaks at 531.68 eV and 529.51 eV in Fig. 11(c) correspond to C=O and Fe_2O_3/Fe_3O_4, respectively (Cui et al., 2017; Tang et al., 2017), the presence of C=O should be attributed to the adsorption of BCQDs on the surface of the carbon steel, while the presence of Fe_2O_3/Fe_3O_4 should be explained by the exposure of the carbon steel sample to air during the test. In addition, the three peaks at 401.19 eV, 399.93 eV and 399.09 eV in Fig. 11(d) are N^+H, *N*-Fe and N—C, respectively. Among them, *N*-Fe is detected because of the chemisorption of BCQDs to the metal surface, while the presence of N^+H demonstrates the physical adsorption of BCQDs to the metal surface (Bentiss et al., 2000). The three peaks at 712.5 eV and 710.4 eV in Fig. 11(e) ascribed to Fe_2O_3/Fe_3O_4 and $FeCl_2$ (Tang et al., 2017), which are caused by the immersion of the carbon steel sheet sample in hydrochloric acid solution and its exposure to air.

3.8. Corrosion inhibition mechanism

The relevant protection mechanism graphic is listed in Fig. 12. Through the analysis of FTIR and XPS, the synthesized BCQDs contains a large number of functional groups including N, O elements and unsaturated bonds, which enable the BCQDs to form coordination bond with Fe elements of Q235 to produce chemisorption. Therefore, the BCQDs can form adsorption films on the surface of Q235 to inhibit the corrosion of the metal. Meanwhile, combined with TEM analysis, the BCQDs are nanoparticles with particle size less than 7 nm. The nanoparticles of BCQDs have high surface energy, which can cause self-aggregation of BCQDs then settle on the metal surface. It can be seen from the OCP tests that the OCP stabilization time grows in electrochemical tests. As shown in Fig. 12, the complementary effect of adsorption and self-aggregation of BCQDs makes the film on the corrosion inhibitor surface dense and thick, showing excellent corrosion inhibition effect.

4. Conclusion

In this experiment, novel BCQDs were successfully synthesized by using grapefruit peels as precursors. The BCQDs were used as green corrosion inhibitors in hydrochloric acid environment, and the following conclusions were drawn through systematic experiments and analysis.

(1) BCQDs were successfully synthesized by hydrothermal method using grapefruit peels as precursors with particle size around 5 nm and C, O and N as the major elements.
(2) The prepared BCQDs are a mixed corrosion inhibitor and the corrosion inhibition efficiency increases with the addition of concentration.
(3) When the temperature is 298 K-328 K, BCQDs can effectively protect the corrosion of Q235 steel in the hydrochloric acid environment, and the corrosion inhibition performance reaches the best (96.5 %) at 308 K.
(4) The protective film formed by BCQDs on the surface of Q235 steel enhances the hydrophobicity of the steel and effectively inhibit the corrosion of steel in hydrochloric acid solution.
(5) BCQDs form protective films on the surface of Q235 steel through chemisorption and self-aggregation deposition.

I would like to declare on behalf of my co-authors that the work described was original research that has not been published previously, and not under consideration for publication elsewhere. All the authors listed have approved the manuscript that is enclosed. To the best of our knowledge, the named authors have no conflict of interest, financial or otherwise.

Declaration of Competing Interest

The authors declare that they have no known competing financial interests or personal relationships that could have appeared to influence the work reported in this paper.

Acknowledgement

This research was supported by Fundamental Research Program of Shanxi Province (No. 20210302124337, No. 202103021224207).

References

Bentiss, F., Traisnel, M., Gengembre, L., Lagrenee, M., 2000. Inhibition of acidic corrosion of mild steel by 3,5-diphenyl-4H-1,2,4-triazole. Appl. Surf. Sci. 161, 194–202.

Cao, S., Liu, D., Wang, T., Ma, A., Liu, C., Zhuang, X., Ding, H., Mamba, B.B., Gui, J., 2021. Nitrogen-doped carbon dots as high-effective inhibitors for carbon steel in acidic medium. Colloids Surf. A Physicochem. Eng. Asp. 616, 126280.

Chin, H.S., Cheong, K.Y., Razak, K.A., 2010. Controlled synthesis of Sb2O3 nanoparticles by chemical reducing method in ethylene glycol. J. Nanopart. Res. 13, 2807–2818.

Cui, M., Ren, S., Xue, Q., Zhao, H., Wang, L., 2017. Carbon dots as new eco-friendly and effective corrosion inhibitor. J. Alloy. Compd. 726, 680–692.

de Damborenea, J., Conde, A., Arenas, M.A., 2014. Corrosion inhibition with rare earth metal compounds in aqueous solutions. Rare Earth-Based Corros. Inhib., 84–116

Dong, Y., Shao, J., Chen, C., Li, H., Wang, R., Chi, Y., Lin, X., Chen, G., 2012. Blue luminescent graphene quantum dots and graphene oxide prepared by tuning the carbonization degree of citric acid. Carbon 50, 4738–4743.

Guo, L., Zhu, M., He, Z., Zhang, R., Kaya, S., Lin, Y., Saji, V.S., 2022. One-pot hydrothermal synthesized nitrogen and sulfur codoped carbon dots for acid corrosion inhibition of Q235 steel. Langmuir 38, 3984–3992.

Guo, L., Zhu, M., Shi, W., Wang, K., Leng, S., Brahmia, A., 2023. Evaluation of the corrosion inhibition behavior of N, S co-doped memory-type carbon dots for mild steel in HCl solution. Mater. Lett. 330, 133403.

Hao, F., Lin, H., Zhou, C., Liu, Y., Li, J., 2011. Bifunctional single-crystalline rutile nanorod decorated heterostructural photoanodes for efficient dye-sensitized solar cells. Phys. Chem. Chem. Phys. 13, 15918–15924.

Hu, Y., Yang, J., Tian, J., Jia, L., Yu, J.-S., 2015. Oxygen-driven, high-efficiency production of nitrogen-doped carbon dots from alkanolamines and their application for two-photon cellular imaging. RSC Adv. 5, 15366–15373.

Hulicova-Jurcakova, D., Seredych, M., Lu, G.Q., Bandosz, T.J., 2009. Combined effect of nitrogen- and oxygen-containing functional groups of microporous activated carbon on its electrochemical performance in supercapacitors. Adv. Funct. Mater. 19, 438–447.

Jiang, D., Chen, Y., Li, N., Li, W., Wang, Z., Zhu, J., Zhang, H., Liu, B., Xu, S., 2015. Synthesis of luminescent graphene quantum dots with high quantum yield and their toxicity study. PLoS One 10, e0144906.

Jiang, K., Sun, S., Zhang, L., Lu, Y., Wu, A., Cai, C., Lin, H., 2015. Red, green, and blue luminescence by carbon dots: full-color emission tuning and multicolor cellular imaging. Angew. Chem. Int. Ed. Engl. 54, 5360–5363.

Lu, W., Qin, X., Liu, S., Chang, G., Zhang, Y., Luo, Y., Asiri, A.M., Al-Youbi, A.O., Sun, X., 2012. Economical, green synthesis of fluorescent carbon nanoparticles and their use as probes for sensitive and selective detection of mercury(II) ions. Anal. Chem. 84, 5351–5357.

Murmu, M., Saha, S.K., Murmu, N.C., Banerjee, P., 2019. Effect of stereochemical conformation into the corrosion inhibitive behaviour of double azomethine based Schiff bases on mild steel surface in 1 mol/L HCl medium: an experimental, density functional theory and molecular dynamics simulation study. Corros. Sci. 146, 134–151.

Nadi, I., Bouanis, M., Benhiba, F., Nohair, K., Nyassi, A., Zarrouk, A., Jama, C., Bentiss, F., 2021. Insights into the inhibition mechanism of 2,5-bis(4-pyridyl)-1,3,4-oxadiazole for carbon steel corrosion in hydrochloric acid pickling via experimental and computational approaches. J. Mol. Liq. 342, 116958.

Niu, F., Ying, Y.-L., Hua, X., Niu, Y., Xu, Y., Long, Y.-T., 2018. Electrochemically generated green-fluorescent N-doped carbon quantum dots for facile monitoring alkaline phosphatase activity based on the Fe3+-mediating ON-OFF-ON-OFF fluorescence principle. Carbon 127, 340–348.

Parthipan, P., Cheng, L., Rajasekar, A., 2021. Glycyrrhiza glabra extract as an eco-friendly inhibitor for microbiologically influenced corrosion of API 5LX carbon steel in oil well produced water environments. J. Mol. Liq. 333, 115952.

Popova, A., Sokolova, E., Raicheva, S., Christov, M., 2003. AC and DC study of the temperature effect on mild steel corrosion in acid media in the presence of benzimidazole derivatives. Corros. Sci. 45, 33–58.

Qiang, Y., Zhang, S., Guo, L., Xu, S., Feng, L., Obot, I.B., Chen, S., 2017. Sodium dodecyl benzene sulfonate as a sustainable inhibitor for zinc corrosion in 26% NH 4 Cl solution. J. Clean. Prod. 152, 17–25.

Qiang, Y., Fu, S., Zhang, S., Chen, S., Zou, X., 2018. Designing and fabricating of single and double alkyl-chain indazole derivatives self-assembled monolayer for corrosion inhibition of copper. Corros. Sci. 140, 111–121.

Qiang, Y., Zhang, S., Tan, B., Chen, S., 2018. Evaluation of Ginkgo leaf extract as an eco-friendly corrosion inhibitor of X70 steel in HCl solution. Corros. Sci. 133, 6–16.

Qiang, Y., Zhang, S., Zhao, H., Tan, B., Wang, L., 2019. Enhanced anticorrosion performance of copper by novel N-doped carbon dots. Corros. Sci. 161, 108193.

Quartarone, G., Battilana, M., Bonaldo, L., Tortato, T., 2008. Investigation of the inhibition effect of indole-3-carboxylic acid on the copper corrosion in 0.5M H2SO4. Corros. Sci. 50, 3467–3474.

Ren, S., Cui, M., Chen, X., Mei, S., Qiang, Y., 2022. Comparative study on corrosion inhibition of N doped and N, S codoped carbon dots for carbon steel in strong acidic solution. J. Colloid Interface Sci. 628, 384–397.

Ren, J., Weber, F., Weigert, F., Wang, Y., Choudhury, S., Xiao, J., Lauermann, I., Resch-Genger, U., Bande, A., Petit, T., 2019. Influence of surface chemistry on optical, chemical and electronic properties of blue luminescent carbon dots. Nanoscale 11, 2056–2064.

Roy, P., Chen, P.-C., Periasamy, A.P., Chen, Y.-N., Chang, H.-T., 2015. Photoluminescent carbon nanodots: synthesis, physicochemical properties and analytical applications. Mater. Today 18, 447–458.

Saha, S.K., Dutta, A., Ghosh, P., Sukul, D., Banerjee, P., 2016. Novel Schiff-base molecules as efficient corrosion inhibitors for mild steel surface in 1 M HCl medium: experimental and theoretical approach. Phys. Chem. Chem. Phys. 18, 17898–17911.

Sanaei, Z., Ramezanzadeh, M., Bahlakeh, G., Ramezanzadeh, B., 2019. Use of Rosa canina fruit extract as a green corrosion inhibitor for mild steel in 1 M HCl solution: a complementary experimental, molecular dynamics and quantum mechanics investigation. J. Ind. Eng. Chem. 69, 18–31.

Song, Y., Zhu, C., Song, J., Li, H., Du, D., Lin, Y., 2017. Drug-derived bright and color-tunable N-doped carbon dots for cell imaging and sensitive detection of Fe(3+) in living cells. ACS Appl. Mater. Interfaces 9, 7399–7405.

Sooksin, S., Promarak, V., Ittisanronnachai, S., Ngeontae, W., 2018. A highly selective fluorescent enhancement sensor for Al3+ based nitrogen-doped carbon dots catalyzed by Fe3+. Sens. Actuators B 262, 720–732.

Sudheer, M.A. Quraishi, Electrochemical and theoretical investigation of triazole derivatives on corrosion inhibition behavior of copper in hydrochloric acid medium, Corrosion Science, 70 (2013) 161-169

Tang, Y., Guo, X.P., Zhang, G.A., 2017. Corrosion behaviour of X65 carbon steel in supercritical-CO 2 containing H 2 O and O 2 in carbon capture and storage (CCS) technology. Corros. Sci. 118, 118–128.

Umoren, S.A., Eduok, U.M., 2016. Application of carbohydrate polymers as corrosion inhibitors for metal substrates in different media: a review. Carbohydr. Polym. 140, 314–341.

Verma, D.K., Khan, F., 2015. Corrosion inhibition of mild steel in hydrochloric acid using extract of glycine max leaves. Res. Chem. Intermed. 42, 3489–3506.

Verma, C., Olasunkanmi, L.O., Ebenso, E.E., Quraishi, M.A., Obot, I. B., 2016. Adsorption behavior of glucosamine-based, pyrimidine-fused heterocycles as green corrosion inhibitors for mild steel: experimental and theoretical studies. J. Phys. Chem. C 120, 11598–11611.

Verma, C., Ebenso, E.E., Quraishi, M.A., 2017. Corrosion inhibitors for ferrous and non-ferrous metals and alloys in ionic sodium chloride solutions: a review. J. Mol. Liq. 248, 927–942.

Wang, W., Lu, Y.C., Huang, H., Feng, J.J., Chen, J.R., Wang, A.J., 2014. Facile synthesis of water-soluble and biocompatible fluorescent nitrogen-doped carbon dots for cell imaging. Analyst 139, 1692–1696.

Wang, B., Wang, Y., Wu, H., Song, X., Guo, X., Zhang, D., Ma, X., Tan, M., 2014. A mitochondria-targeted fluorescent probe based on TPP-conjugated carbon dots for both one- and two-photon fluorescence cell imaging. RSC Adv. 4, 49960–49963.

Wang, X., Yang, H., Wang, F., 2011. An investigation of benzimidazole derivative as corrosion inhibitor for mild steel in different concentration HCl solutions. Corros. Sci. 53, 113–121.

Xu, M., He, G., Li, Z., He, F., Gao, F., Su, Y., Zhang, L., Yang, Z., Zhang, Y., 2014. A green heterogeneous synthesis of N-doped carbon dots and their photoluminescence applications in solid and aqueous states. Nanoscale 6, 10307–10315.

Xu, X., He, L., Long, Y., Pan, S., Liu, H., Yang, J., Hu, X., 2019. S-doped carbon dots capped ZnCdTe quantum dots for ratiometric fluorescence sensing of guanine. Sens. Actuators B 279, 44–52.

Yang, Z., Xu, M., Liu, Y., He, F., Gao, F., Su, Y., Wei, H., Zhang, Y., 2014. Nitrogen-doped, carbon-rich, highly photoluminescent carbon dots from ammonium citrate. Nanoscale 6, 1890–1895.

Yang, D., Ye, Y., Su, Y., Liu, S., Gong, D., Zhao, H., 2019. Functionalization of citric acid-based carbon dots by imidazole toward novel green corrosion inhibitor for carbon steel. J. Clean. Prod. 229, 180–192.

Ye, Y., Zhang, D., Zou, Y., Zhao, H., Chen, H., 2020. A feasible method to improve the protection ability of metal by functionalized carbon dots as environment-friendly corrosion inhibitor. J. Clean. Prod. 264, 121682.

Zheng, X., Zhang, S., Li, W., Gong, M., Yin, L., 2015. Experimental and theoretical studies of two imidazolium-based ionic liquids as inhibitors for mild steel in sulfuric acid solution. Corros. Sci. 95, 168–179.

Zhu, M., Guo, L., He, Z., Marzouki, R., Zhang, R., Berdimurodov, E., 2022. Insights into the newly synthesized N-doped carbon dots for Q235 steel corrosion retardation in acidizing media: a detailed multidimensional study. J. Colloid Interface Sci. 608, 2039–2049.